This is an open access article published under an ACS AuthorChoice License, which permits copying and redistribution of the article or any adaptations for non-commercial purposes.

ACS central science

http://pubs.acs.org/journal/acscii

Research Article

Enhancing the Signaling of GPCRs via Orthosteric Ions

H. C. Stephen Chan,[#] Yueming Xu,[#] Liang Tan,[#] Horst Vogel, Jianjun Cheng,* Dong Wu,* and Shuguang Yuan*

Cite This: *ACS Cent. Sci.* 2020, 6, 274−282

Read Online

ACCESS | Metrics & More | Article Recommendations | Supporting Information

ABSTRACT: G protein-coupled receptors play essential roles in cellular processes such as neuronal signaling, vision, olfaction, tasting, and metabolism. As GPCRs are the most important drug targets, understanding their interactions with ligands is of utmost importance for discovering related new medicines. In many GPCRs, an allosteric sodium ion next to the highly conserved residue $D^{2.50}$ has been proposed to stabilize the inactive receptor state by mediating interactions between transmembrane helices. Here, we probed the existence of internal and functionally important sodium ions in the dopamine D2 receptor, using molecular dynamics simulations. Besides a new sodium ion at the allosteric ligand binding site, we discovered an additional sodium ion, located close to the orthosteric ligand binding site. Through cell-based activation assays, the signaling of D2 receptor with site-specific mutations was tested against a series of chemically modified agonists. We concluded an important structural role of this newly discovered orthosteric sodium ion in modulating the receptor signaling: It enables the coordination of a polar residue in the ligand binding site with an appropriately designed agonist molecule. An identical interaction was also observed in a recently released high-resolution crystal structure of mu-opioid receptor, which was reresolved in this work. Probably because of similar interactions, various metal ions have been found to increase the signaling of many other GPCRs. This unique principle and strategy could be used to optimize the drug activity of GPCR. Our findings open a new mechanistic opportunity of GPCR signaling and help design the next generation of drugs targeting GPCRs.

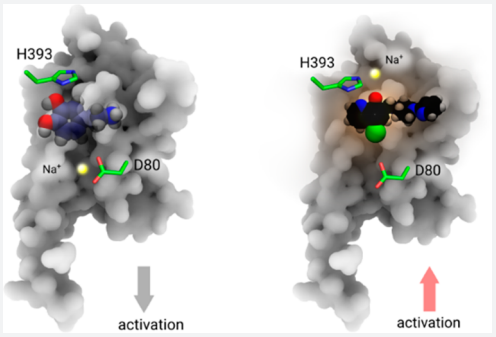

INTRODUCTION

Na^+ ions have been found to influence the functions of many members of class A G protein-coupled receptors (GPCRs), including adrenergic, dopaminergic, adenosine, opioid, and neurotensin receptors.[1−9] For example, the binding of certain ligands to these receptors are known to be sensitive to sodium ions.[1] For the case of dopamine D2 receptor (D2R), the binding of an agonist leads to the coupling of the receptor to $G_{i/o}$ protein that in turn inhibits adenylyl cyclase. At physiological concentration, Na^+ ions decrease the affinities of agonists including the endogenous agonist dopamine but enhance the affinities for some antagonists. The mutation $D80A^{2.50}$ or $D80E^{2.50}$ abolishes Na^+ sensitivity. Several high-resolution crystal structures[1,3,10,11] indicated that residues in the vicinity of $D^{2.50}$ form a distinct Na^+ mediated coordination network. As an example, in both 2.1 Å high-resolution adenosine $A_{2A}R$ and adrenergic β_1AR crystal structures, the side chain oxygen atoms of $D^{2.50}$ and $S^{3.39}$ as well as three additional water molecules coordinate with this conserved Na^+ ion.[12] Such interactions have been proposed to stabilize the inactive state of GPCRs.[1,13,14] This phenomenon was also found by computational simulations.[15,16]

Interestingly, Na^+, as well as other metal ions, have been found elsewhere to modulate ligand binding to GPCRs at physiological conditions.[13,17−27] However, the molecular basis for this unique observation is still unknown. Here, we investigated the molecular mechanism through which the Na^+ ions influence the function of GPCRs. Starting from the recently resolved crystal structure of D2R (pdb: 6CM4),[28] we investigated the allosteric interactions between Na^+ and the agonist MLS1547 in the ligand binding pocket of D2R[13,29] using all-atom molecular dynamics (MD) simulations.[30] Surprisingly, our MD simulations revealed an additional Na^+ ion in the ligand binding site next to extracellular loop 2 (ECL2). This second Na^+ coordinates the interactions between residue $H393^{6.55}$ and MLS1547 via two water molecules. Our findings were further confirmed by functional analysis of the interactions between the rationally designed synthetic analogues of MLS1547 and the mutants of D2R. A systematic analysis of high-resolution GPCR crystal structures also revealed the newly found coordination motif between Na^+ and ligand in other GPCRs. Our findings provide new opportunities for designing novel drugs targeting GPCRs.

Received: December 5, 2019
Published: January 23, 2020

© 2020 American Chemical Society

https://dx.doi.org/10.1021/acscentsci.9b01247
ACS Cent. Sci. 2020, 6, 274−282

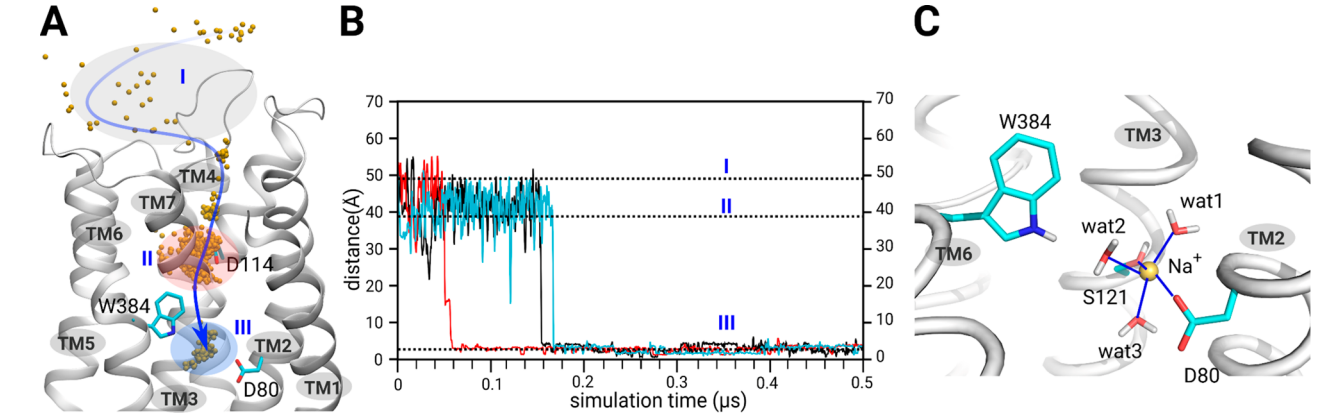

Figure 1. Allosteric Na^+ ion next to $D80^{2.50}$ in D2R. (A) Entrance pathway of a Na^+ ion from the extracellular receptor interface toward the allosteric site $D80^{2.50}$ of apo D2R. Zone I (gray): extracellular receptor interface at which the Na^+ ion is in the bulk environment. Zone II (red): transition zone in the vicinity of $D114^{3.32}$. Zone III (blue): allosteric site in the vicinity of $D80^{2.50}$. Yellow spheres: Na^+ ion positions during MD simulations. (B) Distance between allosteric Na^+ ion and $D80^{2.50}$. (C) The final position of the allosteric Na^+ ion at the end of MD simulations. The oxygen atoms in $D80^{2.50}$ and $S121^{3.39}$ as well as those of three water molecules establish a dedicated coordination network with the allosteric Na^+ ion.

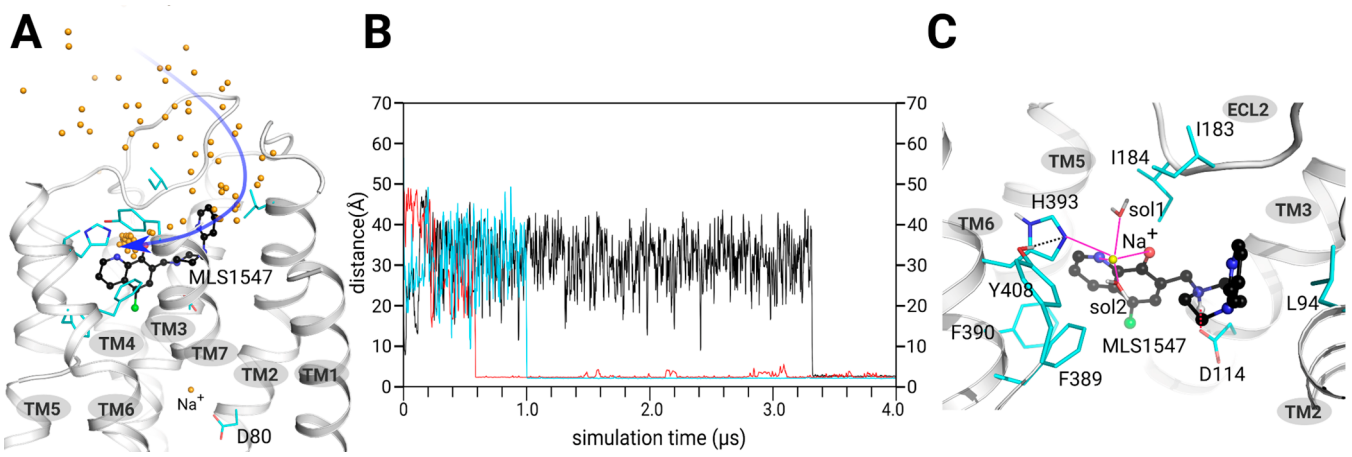

Figure 2. A second Na^+ ion has been found in the orthosteric site of D2R using all-atom long-time MD simulations. (A) The entrance pathway of the orthosteric Na^+ toward agonist molecule MLS1547. Yellow spheres: Na^+ ion trajectories in the MD simulations. Black ball-and-stick: MLS1547. (B) The distance between orthosteric Na^+ ion and $H393^{6.55}$ (C) The final position of the orthosteric Na^+ ion at the end of MD simulations. MLS1547 and $H393^{6.55}$ as well as two water molecules establish a dedicated coordination network with the orthosteric Na^+ ion.

RESULTS AND DISCUSSION

Allosteric Na^+ Ion Next to $D80^{2.50}$ in apo D2R. The allosteric Na^+ ion next to $D^{2.50}$ has been observed in several crystal structures of GPCRs, and is considered to play an essential role in GPCR signaling.[1,31] Although no allosteric Na^+ ion is observed in the recently published 2.8 Å resolution D2R crystal structure (pdb: 6CM4),[28] the signaling of D2R has been shown to depend critically on Na^+ ions.[20,23,32,33] This raises a question whether an allosteric Na^+ ion next to $D^{2.50}$ may actually be present in the D2R also, but the resolution of the mentioned crystal structure might be too low to detect the electron density of a sodium ion. To evaluate whether an allosteric Na^+ ion could exist in D2R, we first performed 3 × 0.5 μs all-atom MD simulations for apo D2R, based on its crystal structure (pdb: 6CM4)[28] (Figure 1). The initial D2R structure did not contain any intrinsic sodium ion, and the sodium ions were present in the extramembrane bulk medium for crystal growth. Interestingly, an allosteric Na^+ ion was found in all three simulations (Figure 1A and Movie 1). During the initial 0.1 μs simulation period (Figure 1B), Na^+ ions fluctuated in the extracellular bulk environment (zone I). During 0.1−0.2 μs time scale, a Na^+ ion moved to $D114^{3.32}$ and formed a transient ionic interaction. After about 0.2 μs, this Na^+ ion diffused deeper into the receptor in the vicinity of $D80^{2.50}$ (Figure 1B) and was finally stabilized in this region until the end of the MD simulations. At this position the Na^+ ion formed a stable coordination complex with the side chain oxygen atoms of $D80^{2.50}$ and $S121^{3.39}$ of apo D2R together with three additional water molecules (Figure 1C). This feature is in good agreement with allosteric Na^+ ions found in several high-resolution crystal structures of other GPCRs (Figure S1).

A New Orthosteric Na^+ Ion in the Extracellular Region of D2R. To study the role of Na^+ ions within the interaction of a potent agonist, for example, MLS1547, and D2R at the atomic level, we first computationally constructed the D2R-MLS1547 complex by protein−ligand docking. The binding model was identical to that of the dopamine D3 receptor (D3R) crystal structure (pdb: 3PBL, Figure S2). Then, we submitted the D2R-MLS1547 complex to 3 × 4.0 μs all-atom MD simulations (Figure 2). MLS1547 was stable

https://dx.doi.org/10.1021/acscentsci.9b01247
ACS Cent. Sci. 2020, 6, 274−282

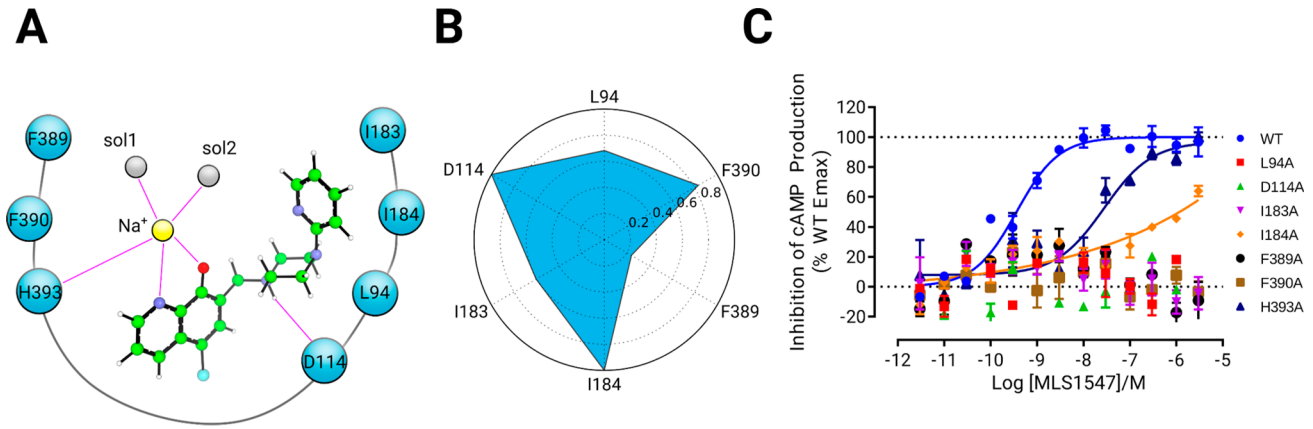

Figure 3. Interaction fingerprint between distinct residues in D2R and MLS1547. (A) The 2D interaction diagram of D2R in complex with MLS1547. Green ball-and-stick: MLS1547. (B) The interaction fingerprint between residues in D2R and MLS1547. It represents the interaction frequency during the MD simulations. (C) Arrestin recruitment for D2R variants showing mutations on key residues predicted by MD simulations. All mutated receptors show noticeably decreased signaling.

Table 1. Activities of Agonist MLS1547 against Different D2R variants (EC_{50}, nM)

	WT	L94A	D114A	I83A	I84A	F389A	F390A	H393A
G protein	290 ± 90	inactive	inactive	inactive	9000 ± 7600	inactive	inactive	inactive
β-arrestin	250 ± 60	inactive	inactive	inactive	2500 ± 600	inactive	inactive	inactive

during MD simulations as indicated by its RMSD (root-mean-square deviation) (Figure S3). Because we observed also for this case the existence of the allosteric Na^+ ion next to $D80^{2.50}$, we kept it in all subsequent MD simulations from the beginning, especially considering residue $D^{2.50}$ is deprotonated at the initial activation stage of GPCRs.[1,34] Interestingly, we found in these simulations a second Na^+ ion captured in the orthosteric site next to the agonist molecule, forming coordination with both MLS1547 and D2R at 1.0−3.2 μs time scale (Figure 2). Quantum mechanics calculation indicated that the −OH group is deprotonated in the quinolin-8-ol moiety of MLS1547, due to the presence of the strong electronegative -Cl atom in the *para* position. Here, the nitrogen atom and the negatively charged oxygen established a coordination with this orthosteric Na^+ ion. Moreover, $H393^{6.55}$ together with two water molecules from the bulk environment formed coordination bonds with the Na^+ ion (Figure 2C and Figure 3A).

We then performed a protein−ligand interaction fingerprint (IFP) analysis on the generated MD simulation trajectories. IFP is a very useful method to quantify the interaction frequency between a protein and a ligand of interest.[35−38] The analysis identifies which residues are most important for a specific protein−ligand interaction network. Besides the coordinating interaction with residue $H393^{6.55}$, IFP analysis on the MD simulation trajectories indicated a few additional interactions of MLS1547 within the receptor including (1) face-to-side $\pi-\pi$ stacking interactions with the two aromatic residues $F389^{6.51}$ and $F390^{6.52}$, (2) ionic interactions with $D114^{3.32}$, and finally (3) hydrophobic interactions with the residues $I183^{ECL2}$ and $I184^{ECL2}$ in the ECL2 loop (Figure 3B).

To validate this newly discovered binding mode, we modified the D2R site specifically on the key residues indicated by the IFP analysis, and tested the activation of wildtype and mutant proteins by functional analyses. The EC_{50} value for wildtype receptor activation by MLS1547 was 630 nM for G protein signaling and 250 nM for arrestin signaling. Interestingly, all mutations had a substantial influence on the agonist induced receptor activation (Figure 3C and Table-1). Specifically, mutation variants $I83^{ECL2}A$, $L94^{2.64}A$, $D114^{3.32}$ A, $F389^{6.51}A$, and $F390^{6.52}A$ completely abolished the activations of both G protein and arrestin. Interestingly, the mutation of $H393^{6.55}A$ led to MLS1547 completely inactive toward arrestin signaling, whereas it was still active against G protein signaling (EC_{50} = 350 nM). In contrast, mutant $I84^{ECL2}A$ was completely inactive toward G protein signaling but still had weak activity toward arrestin signaling (EC_{50} = 2500 nM). These results echoed the unique binding mode of MLS1547 in the D2R complex.

To further validate our findings, we performed biological testing of dopamine against D2R (Table-S1 and Figure S4). For this case, the interaction between the orthosteric Na^+ and dopamine is missing, as indicated by docking (Figure S5). Previous studies found a similar binding mode for dopamine against D2R.[39,40] These findings were confirmed by the observation that mutation $H393^{6.55}A$ does not show significant influences on dopamine's activity: 970 nM (wildtype) vs 1002 nM (mutant).

In contrast, MLS1547 abolished its activity completely. The orthosteric Na^+ ion coordinates agonist induced activation of D2R. As indicated in Figure 3A, a Na^+ ion is involved in the interaction network of the agonist MLS1547 with residues in the orthosteric binding pocket of D2R and modulates the activation of the receptor. For the stability of the ligand−receptor complex, polar groups in the agonist molecule play a central role.

To further investigate how the chemical structure of the agonist determines the unique binding mode, we synthesized several derivatives of MLS1547 (Figure 4 and Table-S2). We first prepared 5-substituted quinolin-8-ol (see Materials and Methods). In the variant MLS-d1, a fluorine replaced the chlorine in MLS1547. The strong electronegativity of F decreased substantially the pK_a value of the hydroxyl group of MLS1547 from 6.3 to 4.2 (Table-S2). Consequently, the group

https://dx.doi.org/10.1021/acscentsci.9b01247
ACS Cent. Sci. 2020, 6, 274−282

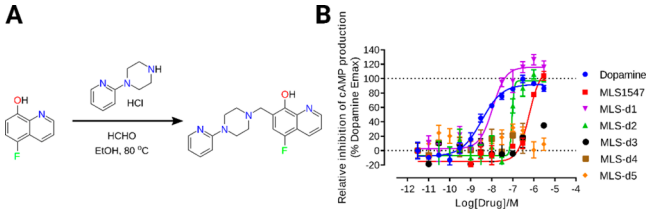

Figure 4. Synthesis and biological activity of MLS1547 derivatives. (A) Scheme for synthesis of compound MLS-d1. (B) Activation of D2R mediated signaling induced by dopamine, MLS1547- and MLS1547-derivatives.

is deprotonated facilitating the interaction with the orthosteric Na^+ ion (Figure 3A). This in turn improved the activation of the G protein with a decrease in EC_{50} values by almost 34 times, to 18.6 nM (Table-S2). Interestingly, the removal of Cl in MLS-d2 increased the pK_a only slightly to 6.4 ± 0.7, but resulted also in an improved activation of G protein as shown by the EC_{50} values of 95 nM (Table-S2). We noticed that the activity of MLS-d2 is even slightly higher than MLS1547. Probably the presence of a -Cl might impose allosteric effects in the binding site as shown in Figure S6. Moreover, the relatively large -Cl is a little bit closer to the negatively charged $D114^{3.32}$, inducing electrostatic repulsions. We also prepared MLS-d3, in which a bromine replaced the chlorine. In turn, the pK_a value increased to 7.4 and the compound was completely inactive (MLS-d3, Table-S2). Moreover, introducing a nitro group in the para position of -OH decreased the pK_a substantially to 3.4 (MLS-d4, Table-S2). However, the nitro group is too big to be accommodated in the binding pocket of D2R and therefore this compound did not show activation of G-protein and arrestin (Figure S6). Furthermore, one of the oxygen atoms in the nitro group was too close to the oxygen atom of $D114^{3.32}$, which might lead to strong unfavorable electrostatic repulsion (Figure S6). In addition, we prepared compound MLS-d5, in which the N atom in quinolin-8-ol ring was replaced by a -CH group. The loss of coordination possibility led MLS-d5 to be completely inactive. Moreover, the estimated relative binding energies of MLS1547 variants correlate well with their EC_{50} values (Table-S2). This implies that MLS1547 and certain variants enhance the signaling by increasing the ligand binding through unique ion-coordinating interactions (Figures 2C and 3A).

An Allosteric Ion in the Crystal Structure of μ-Opioid Receptor and Potential Application in Other GPCRs. A recent high-resolution crystal structure of μ-opioid receptor (μOR, PDB: 5C1M) showed that there is an "unidentified electron density map" between agonist BU72 and a His residue of μOR.[41] We tried filling this part of the electron density map with different ions, including Li, Na, Mg, Ni, and Zn. We found that only Mg fit perfectly to this region (Figures S7 and S8): the F_O-F_C electron density map was clean and the $2F_O-F_C$ map matched model very well, whereas all other ions always result in either negative Fo−Fc maps (ions are too large to fit in) or positive Fo−Fc maps (ions are too small to fit in). Specifically, the Mg coordinates with both the ligand BU72 and μOR, which is identical to the interactions in this work for D2R. More importantly, Mg was confirmed to enhance the signaling of μOR in other previous work.[26,27] This further strongly supported that modulating the ligand binding via an orthosteric ion could be a universal strategy for GPCR ligand design.

To further validate whether similar interactions might happen in other GPCRs, a detailed inspection of family A GPCR structures shows that His is a frequent residue in TM6 of GPCRs (Figure S9). Considering that the ligand binding pocket of many family A GPCRs is very large, it is possible that a His in TM6 in other receptors might establish similar interaction networks as reported in the present work. Indeed, the signaling of many other GPCRs have been found to be enhanced by various metal ions elsewhere,[15−21] probably because of the similar coordinating interactions as well.

Conclusion and Perspectives. An allosteric sodium ion has been observed in several high-resolution GPCR structures including $A_{2A}R$, D4R, β_1AR, and others.[1,3−5] The binding site of the allosteric sodium ion is located next to the highly conserved residue $D^{2.50}$ in the inner space of the TM region in family A GPCRs. The specific coordination of the allosteric sodium ion strengthen links between different TM helices to enhance the stability of the inactive state of the particular receptors (Figure 5, left panel).[1,2,14]

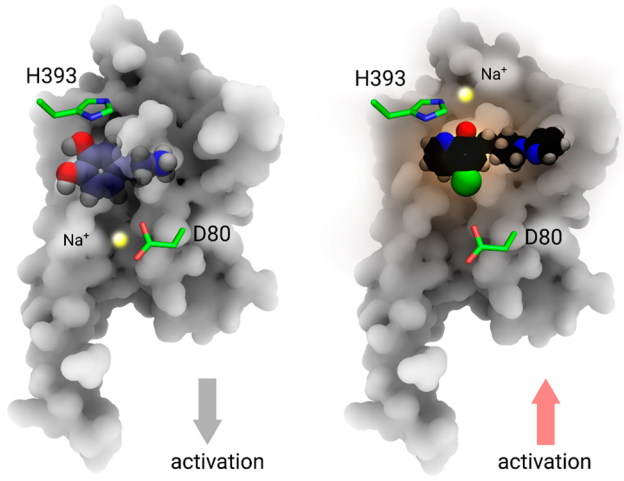

Figure 5. Two different roles of Na^+ in D2 receptor activation. Left panel: an allosteric Na^+ (yellow sphere) stabilizes the inactive state of receptor. Blue ball-and-sphere: dopamine molecule. Right panel: an orthosteric Na^+ enhances the activation of receptor via a coordinating interaction with both $H393^{6.55}$ and agonist molecule MLS1547 (black ball-and-stick).

Using all-atom MD simulations of apo-D2R, we have identified the potential existence of an allosteric Na^+ ion next to $D^{2.50}$, which resembles allosteric Na^+ ions found in crystal structures of other GPCRs.[1,2,14,32] For the case of the D2R in complex with an agonist, the MD simulations revealed in an additional Na^+ ion located in the orthosteric ligand binding site in the extracellular region (Figure 5, right panel). Different from previous findings, this newly discovered Na^+ enhances ligand binding by coordinating with both a His amino acid in TM6 of D2R and a negatively charged group in the ligand (Figure 2C and 3A), which in turn facilitates signaling of agonist molecules. Both site-specific mutagenesis experiments and structure−activity relationship (SAR) studies are in excellent agreement with our proposed model. The complementary site-specific mutations in the ligand binding pocket of the D2R and the properties of the modified agonists are also in agreement with the proposed role of allosteric and orthosteric Na^+ ions for the activation of the D2R. An identical interaction

https://dx.doi.org/10.1021/acscentsci.9b01247
ACS Cent. Sci. 2020, 6, 274−282

was also observed in the high-resolution crystal structure of μOR by reresolving the structure.

Our findings reveal details of the role of sodium ions as well as other metal ions in GPCR signaling. These findings could be used to design unique GPCR drug molecules or to optimize ligand properties.

MATERIALS AND METHODS

Tango Arrestin Recruitment Assay. The D2R-arrestin recruitment assays were performed as previously described.[42] Briefly, HTLA cells expressing the TEV fused-β-arrestin2 were transfected with 1 μg D2R wild-type or mutant DNA per 10 cm dish in 10% dialyzed FBS DMEM. The next day, cells were plated into white 384-well plates at a density of 15 000 cells per well in 20 μL of 1% dialyzed FBS DMEM. After 6 h cells were stimulated with drugs ranging in concentration from 30 μM to 1 pM diluted in drug buffer (20 mM HEPES, 1X HBSS, 0.1% BSA, 0.01% ascorbic acid, pH 7.4) at a 3-fold concentration. After overnight incubation at 37 °C and 5% CO_2, media was decanted and 20 μL of BriteGlo (Promega, after 1:20 dilution) was added per well. After 20 min, plates were read on an EnVision (PerkinElmer) at 1 ms per well. Luminescence counts per second (LCPS) were plotted as a function of drug concentration and analyzed using Graphpad Prism 8.0. Data were normalized to percent WT response, which was present in every experiment.

Split Luciferase Biosensor cAMP Assay for Measuring Activation of Gi Protein. To determine G_i-GPCR mediated cAMP production, we used Promega's split luciferase based GloSensor cAMP biosensor technology. On the first day, 1 μg of target receptor DNA and 1 μg of GloSensor cAMP DNA were cotransfected into ATCC HEK 293T by Lipofectamine 2000. After a minimum incubation of 6 h, cells are seeded into 384-well white clear bottom cell culture plates with F-12 supplemented with 10% FBS at a density of 10−15 000 cells in 40 μL of medium per well. The assay was carried out after overnight incubation. On the day of the assay, supernatant was removed from the plates. Wells are loaded for 60 min at 37°C with 20 μL of 2 mg/mL luciferin prepared in HBSS, pH 7.4. All the following steps were carried out at room temperature. To measure agonist activity at D2R, 10 μL fo 4× test drug solution was added for 15 min before addition of 10 μL of forskolin at a final concentration of 20 μM, followed by counting of the plate for chemiluminescence after 15 min.

Organic Synthesis of Compounds. *Experimental Procedures for Organic Synthesis.* All commercial chemicals and solvents were used as obtained from the manufacturer without further purification. Flash chromatography were run on 200−300 mesh silica gel using a Teledyne CombiFlash instrument. ^{1}H NMR spectra were recorded on a Bruker AVANCE-III spectrometer at 800 MHz. ^{13}C NMR spectra were recorded on a Bruker AVANCE-III spectrometer at 151 MHz. NMR chemical shifts were reported in δ (ppm) using residual solvent peaks as standards ($CDCl_3$−7.26 (H), 77.16 (C); CD_3OD−3.31 (H), 49.00 (C); DMSO-d_6−2.50 (H), 39.52 (C)). Mass spectra were measured using an LCMS-IT-TOF (Shimadzu) mass spectrometer in ESI mode. The purity of all final compounds (>95%) were determined by analytical HPLC (Shim-pack GIST C18 column (250 × 4.6 mm, particle size 5 μM); 0.05% TFA in H_2O/0.05% TFA in MeOH gradient eluting system; flow rate = 1.0 mL/min). Preparative HPLC was conducted using Shimadzu HPLC system (Shim-pack GIST C18 column (250 × 20 mm, particle size 5 μM); H_2O/MeOH gradient eluting system; flow rate = 10.0 mL/min).

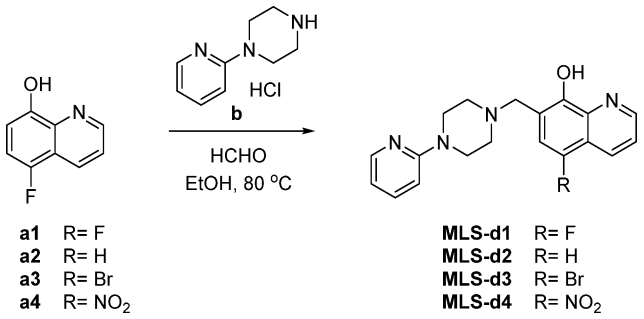

*5-Fluoro-7-((4-(pyridin-2-yl)piperazin-1-yl)methyl)-quinolin-8-ol (**MLS-d1**).* To a mixture of compound **a1** (300 mg, 1.84 mmol) in anhydrous EtOH (20 mL) was added 1-(pyridin-2-yl)piperazine hydrochloride **b** (550 mg, 2.76 mmol) and formaldehyde (37% aqueous solution, 0.30 mL, 4.05 mmol). The mixture was stirred at 80 °C for 12 h under N_2. Then the pH of the mixture was adjusted to 8.0 by saturated aqueous $NaHCO_3$. The mixture was then extracted with ethyl acetate (30 mL × 2). The combined extracts were washed with brine (10 mL × 2), dried over anhydrous Na_2SO_4, and concentrated in vacuum to give a residue. The residue was purified by silica gel chromatography (petroleum ether/ethyl acetate = 1/0 to 1/1) to obtain a yellow solid, which was stirred in hexane (2 mL) at room temperature for 2 h. Compound **MLS-d1** (110 mg, 17.7% yield) was collected by filtration as a white solid. ^{1}H NMR (800 MHz, CD_3OD) δ 8.86 (d, J = 4.1 Hz, 1H), 8.43 (d, J = 8.5 Hz, 1H), 8.08 (d, J = 5.1 Hz, 1H), 7.60−7.53 (m, 2H), 7.22 (d, J = 10.4 Hz, 1H), 6.83 (d, J = 8.6 Hz, 1H), 6.68 (t, J = 6.1 Hz, 1H), 3.92 (s, 2H), 3.58 (t, J = 5.1 Hz, 4H), 2.72 (t, J = 5.1 Hz, 4H). ^{13}C NMR (151 MHz, DMSO-d_6) δ 159.0, 149.3, 149.2 (d, J = 243.3 Hz), 147.8 (d, J = 3.1 Hz), 147.6, 137.9 (d, J = 3.1 Hz), 137.5, 129.0, 121.9, 119.5 (d, J = 6.6 Hz), 117.5 (d, J = 18.2 Hz), 113.0, 111.9 (d, J = 20.3 Hz), 107.1, 55.9, 52.4 (2C), 44.7 (2C). HRMS (m/z): $[M + H]^+$ calculated for $C_{19}H_{20}FN_4O^+$ 339.1616, found 339.1623.

*7-((4-(Pyridin-2-yl)piperazin-1-yl)methyl)quinolin-8-ol (**MLS-d2**).* To a mixture of compound **a2** (250 mg, 1.72 mmol) in anhydrous EtOH (20 mL) was added 1-(pyridin-2-yl)piperazine hydrochloride **b** (513.4 mg, 2.58 mmol) and formaldehyde (37% aqueous solution, 0.28 mL, 3.79 mmol). The reaction mixture was stirred at 80 °C for 12 h under N_2. Then the pH of the mixture was adjusted to 8.0 with saturated aqueous $NaHCO_3$. The mixture was then extracted with ethyl acetate (200 mL × 2). The combined organic extracts were washed with brine (100 mL × 2), dried over anhydrous Na_2SO_4, and concentrated in vacuum to give a residue, which was purified by preparative HPLC to give compound **MLS-d2** (45.7 mg, 8.3% yield) as a gray solid. ^{1}H NMR (800 MHz, CD_3OD) δ 8.79 (d, J = 3.1 Hz, 1H), 8.24 (dd, J = 8.3, 1.6 Hz, 1H), 8.08 (dd, J = 5.1, 1.9 Hz, 1H), 7.57−7.54 (m, 1H), 7.48 (dd, J = 8.3, 4.1 Hz, 1H), 7.40 (d, J = 8.3 Hz, 1H), 7.37 (d, J = 8.3 Hz, 1H), 6.82 (d, J = 8.6 Hz, 1H), 6.68 (dd, J = 7.1, 5.0 Hz, 1H), 3.95 (s, 2H), 3.58 (t, J = 5.2 Hz, 4H), 2.73 (t, J = 5.0 Hz, 4H). ^{13}C NMR (151 MHz, DMSO-d_6) δ 159.0, 151.3, 148.2, 147.6, 138.2, 137.5, 136.0, 129.1, 127.7, 121.6, 119.7, 117.0, 113.0, 107.1, 56.3, 52.4 (2C), 44.7 (2C). HRMS (m/z): $[M + H]^+$ calculated for $C_{19}H_{21}N_4O^+$ 321.1710, found 321.1713.

https://dx.doi.org/10.1021/acscentsci.9b01247
ACS Cent. Sci. 2020, 6, 274−282

*5-Bromo-7-((4-(pyridin-2-yl)piperazin-1-yl)methyl)-quinolin-8-ol (**MLS-d3**).* To a mixture of **a3** (250 mg, 1.12 mmol) in anhydrous EtOH (20 mL) was added 1-(pyridin-2-yl)piperazine hydrochloride **b** (334 mg, 1.68 mmol) and formaldehyde (37% aqueous solution, 0.18 mL, 2.45 mmol). The mixture was stirred at 80 °C for 12 h under N_2. Then the pH was adjusted to 8.0 by saturated aqueous $NaHCO_3$. The mixture was then extracted with ethyl acetate (20 mL × 2). The combined extracts were washed with brine (10 mL × 2), dried over anhydrous Na_2SO_4, and concentrated in vacuum to give a residue, which was purified by preparative HPLC to give compound **MLS-d3** (21.0 mg, 5.8% yield) as a yellow solid. ^{1}H NMR (800 MHz, CD_3OD) δ 8.85 (s, 1H), 8.51 (dd, J = 8.5, 1.5 Hz, 1H), 8.08 (dd, J = 5.1, 1.4 Hz, 1H), 7.77 (s, 1H), 7.63 (dd, J = 8.5, 4.2 Hz, 1H), 7.58−7.53 (m, 1H), 6.83 (d, J = 8.6 Hz, 1H), 6.68 (dd, J = 7.1, 5.0 Hz, 1H), 3.93 (s, 2H), 3.58 (t, J = 5.1 Hz, 4H), 2.73 (t, J = 5.1 Hz, 4H). ^{13}C NMR (151 MHz, DMSO-d_6) δ 159.0, 151.6, 149.0, 147.6, 139.1, 137.5, 134.9, 132.2, 126.2, 123.1, 121.3, 113.0, 108.1, 107.1, 55.6, 52.4 (2C), 44.7 (2C). HRMS (m/z): $[M + H]^+$ calculated for $C_{19}H_{20}BrN_4O^+$ 399.0815, found 399.0827.

*5-Nitro-7-((4-(pyridin-2-yl)piperazin-1-yl)methyl)quinolin-8-ol (**MLS-d4**).* To a mixture of 1-(pyridin-2-yl)piperazine hydrochloride **b** (0.88 g, 4.41 mmol) in pyridine (3.0 mL) and H_2O (3.0 mL) was added formaldehyde (37% aqueous solution, 0.36 mL, 4.41 mmol) at 50 °C. The reaction mixture was stirred at the same temperature for 5 min, and then added to a solution of **a4** (400 mg, 2.10 mmol) in pyridine (10.0 mL) at 50 °C under N_2. The reaction mixture was stirred at 50 °C for 2 h, and then ethyl acetate (20 mL) was added at room temperature to give a yellow solid, which was collected by filtration and recrystallized from ethanol (20 mL) to give compound **MLS-d4** (100 mg, 13.0% yield) as a yellow solid. ^{1}H NMR (800 MHz, DMSO-d_6) δ 9.19 (d, J = 8.6 Hz, 1H), 8.75 (d, J = 3.2 Hz, 1H), 8.58 (s, 1H), 8.13 (dd, J = 4.7, 1.4 Hz, 1H), 7.67 (dd, J = 8.7, 4.0 Hz, 1H), 7.58−7.53 (m, 1H), 6.87 (d, J = 8.6 Hz, 1H), 6.68 (dd, J = 6.9, 5.0 Hz, 1H), 4.06 (s, 2H), 3.70 (t, J = 5.0 Hz, 4H), 3.02 (t, J = 5.0 Hz, 4H). ^{13}C NMR (151 MHz, DMSO-d_6) δ 169.3, 158.5, 147.6, 147.0, 139.9, 137.8, 132.7, 132.2, 127.1, 124.5, 124.4, 115.6, 113.6, 107.5, 56.1, 51.7 (2C), 43.1 (2C). HRMS (m/z): $[M + H]^+$ calculated for $C_{19}H_{20}N_5O_3^+$ 366.1561, found 366.1556.

Synthesis of a4. *5-Nitrosoquinolin-8-ol (**a5**).* Concentrated H_2SO_4 (3 mL) was added slowly into H_2O (65 mL),

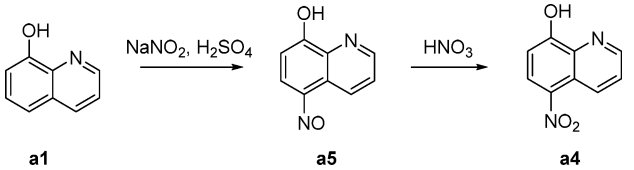

and the resulting solution was stirred vigorously at 15−18 °C. Compound **a1** (7.4 g, 50 mmol) was added. A solution of $NaNO_2$ (3.7 g, 54 mmol) in H_2O (7 mL) was added dropwise over 30 min. The reaction mixture was stirred at 18−20 °C for 3 h, and then 20% NaOH was added slowly to adjust to pH 10−11, with the temperature kept below 25 °C. The mixture was filtered, and the filtrate was acidified to pH 5−6 with glacial acetic acid. The resulting solid was collected by filtration, washed with H_2O (100 mL), and dried to give compound **a5** (8.4 g, 95% yield), which was used for the next step without further purification.

*5-Nitroquinolin-8-ol (**a4**).* Fuming HNO_3 (0.10 mL) was added dropwise to the suspension of compound **a5** (7.5 g, 43 mmol) in acetic acid (23 mL), and the reaction mixture was stirred at 20 °C for 2 h. The mixture was basified at the temperature not exceeding 25 °C using 20% NaOH to pH 10−11, filtered, then the filtrate was acidified to pH 5−6 with glacial acetic acid. The formed precipitate was filtered, washed with H_2O (100 mL), acetone (15 mL × 2), and then dried to give the compound **a4** (5.7 g, 70% yield).

Loop Modeling and Structural Preparations. *Loop Filling and Refinements.* The published crystal structures of D2R comprised the engineered receptors and inserted proteins in the intracellular loop ICL2 to facilitate crystallization. Before starting MD simulations, we removed the corresponding inserted proteins from the D2R crystal structures and used the loop refinement protocol in Modeler[43] V9.10 to reconstruct and refine the ICL2 region. A total of 10 000 loops were generated for each receptor and the conformation with the lowest DOPE (Discrete Optimized Protein Energy) score was chosen for receptor construction. Repaired models were submitted to Rosetta V3.4 for loop refinement with kinematic loop modeling methods.[44] Kinematic closure (KIC) is an analytical calculation procedure inspired by robotics techniques for rapidly determining possible conformations of linked objects subject to constraints. In the Rosetta KIC implementation, 2N − 6 backbone torsions of an N-residue peptide segment (called nonpivot torsions) were set to values drawn randomly from the Ramachandran space of each residue type, and the remaining 6 phi/psi torsions (called pivot torsions) were solved analytically by KIC.

Protein Structure Preparations. All protein models were prepared in Schrodinger suite software under the OPLS_2005 force field.[45] Hydrogen atoms were added to the repaired crystal structures at physiological pH (7.4) with the PROPKA[46] tool to optimize the hydrogen bond network provided by the Protein Preparation tool in Schrodinger. The highly conserved $D80^{2.50}$ has been found to be deprotonated. Since we only study the initial binding process of D2R, D2.50 in GPCR is always in a deprotnated state as indicated by previous study.[34,47] Thus, we kept the deprotonated state for $D80^{2.50}$ during MD simulations. Constrained energy minimizations were carried out on the full-atomic models, until the RMSD of heavy atoms coveraged to 0.4 Å.

Ligand Structure Preparations. All ligand structures were prepared in Schrodinger software. The LigPrep module in Schrodinger 2015 suite software was introduced for geometric optimization by using the OPLS_2005 force field. The ionization state of ligands was calculated with the Epik[48] tool employing Hammett and Taft methods in combination with ionization and tautomerization tools.[48]

Molecular Dynamics Simulations. Membrane systems were built using the membrane building tool g_membed[49] in Gromacs with the receptor crystal structure prealigned in the OPM (Orientations of Proteins in Membranes) database.[50] Pre-equilibrated 120 POPC lipids coupled with 8000 TIP3P water molecules in a box ∼73 × 73 × 92 Å^3 were used to build the protein/membrane/water system. We modeled the protein, lipids, water, and ions using the CHARMM36m force field.[51] Ligands were assigned with CHARMM CgenFF force field.[52] Ligand geometry was submitted to the GAUSSIAN 09 program[53] for optimization at the Hartree−Fock 6-31G* level when generating force field parameters. The system was gradually heated from 0 to 310 K followed by a 1 ns initial

https://dx.doi.org/10.1021/acscentsci.9b01247
ACS Cent. Sci. 2020, 6, 274−282

equilibration at constant volume with the temperature set at 310 K. The backbone of a particular protein and the heavy atoms of a particular ligand were restrained during the equilibration steps. All bond lengths to hydrogen atoms were constrained with M-SHAKE. Nonbonded interactions were treated using the force switch of 10−12 Å. Long-range electrostatic interactions were computed by the Particle Mesh Ewald (PME) summation scheme. All MD simulations were done in Gromacs.[54] The simulation parameter files were obtained from CHARMM-GUI Web site.[55] Figures were prepared in PyMOL and Inkscape.[56]

For the simulation of the apo-GPCR forms, all Na^+ ions were presented in the bulk environment. The allosteric Na^+ ions diffused into the inner space of D2R at a certain stage of the MD simulations. In the simulation of D2R in complex with MLS1547, we kept a Na^+ ion at the allosteric site next to $D^{2.50}$, which is sampled in the simulation of apo GPCR forms.

Identifying a Mg^{2+} in the μOR crystal structure. Both coordinates, electron density map and topology files for PDB: 5CM1 were obtained from PDB database. We resolved the structure again with programs Phenix[57] and Coot.[58] The geometry of molecule BU72 was optimized using quantum mechanical (QM) method at level B3LYP/6-31G* by Jaguar[59] in Schrodinger software[60] prior to the refinement. The Phenix was used for metal ion identification.[57]

■ ASSOCIATED CONTENT

Supporting Information

The Supporting Information is available free of charge at https://pubs.acs.org/doi/10.1021/acscentsci.9b01247.

MD simulations data (PDF)

Movie 1: An allosteric sodium ion next to D2.50 was captured by MD simulations. (MP4)

Movie 2: A new orthosteric sodium ion, which established coordinations with both receptor and ligand, was captured by MD simulations. (MP4)

■ AUTHOR INFORMATION

Corresponding Authors

Jianjun Cheng − *iHuman Institute, ShanghaiTech University, Shanghai 201210, China;* orcid.org/0000-0001-6065-2682; Email: chengjj@shanghaitech.edu.cn

Dong Wu − *iHuman Institute, ShanghaiTech University, Shanghai 201210, China*; Email: wudong@shanghaitech.edu.cn

Shuguang Yuan − *Shenzhen Institutes of Advanced Technology, Chinese Academy of Sciences, Shenzhen 518055, China;* orcid.org/0000-0001-9858-4742; Email: shuguang.yuan@siat.ac.cn

Authors

H. C. Stephen Chan − *Shenzhen Institutes of Advanced Technology, Chinese Academy of Sciences, Shenzhen 518055, China*

Yueming Xu − *iHuman Institute, ShanghaiTech University, Shanghai 201210, China*

Liang Tan − *iHuman Institute, ShanghaiTech University, Shanghai 201210, China*

Horst Vogel − *Shenzhen Institutes of Advanced Technology, Chinese Academy of Sciences, Shenzhen 518055, China; Institute of Chemical Sciences and Engineering, Ecole Polytechnique Fédérale de Lausanne (EPFL), Lausanne 1015, Switzerland;* orcid.org/0000-0001-9695-8894

Complete contact information is available at: https://pubs.acs.org/10.1021/acscentsci.9b01247

Author Contributions

#(H.C.S.C., Y.X., L.T.) These authors contributed equally to this work. S.Y. initialized and led this work.

Notes

The authors declare the following competing financial interest(s): H.C.S.C., H.V., and S.Y. are the cofounders of AlphaMol Science Ltd.

■ ACKNOWLEDGMENTS

We would like to thank Fei Li from iHuman Institute for repeating some functional analyses. Our calculations were supported by the Interdisciplinary Centre for Mathematical and Computational Modelling in Warsaw (grant nos. GB70-3 & GB71-3). This project was financially supported by the internal funding of Shenzhen Institutes of Advanced Technology, CAS.

■ ABBREVIATIONS

GPCR, G protein-coupled receptor; MD, molecular dynamics; ECL2, extracellular loop 2

■ REFERENCES

(1) Katritch, V.; Fenalti, G.; Abola, E. E.; Roth, B. L.; Cherezov, V.; Stevens, R. C. Allosteric sodium in class A GPCR signaling. *Trends Biochem. Sci.* **2014**, *39* (5), 233.

(2) Gutierrez-de-Teran, H.; Massink, A.; Rodriguez, D.; Liu, W.; Han, G. W.; Joseph, J. S.; Katritch, I.; Heitman, L. H.; Xia, L.; Ijzerman, A. P.; et al. The role of a sodium ion binding site in the allosteric modulation of the A(2A) adenosine G protein-coupled receptor. *Structure* **2013**, *21* (12), 2175.

(3) Miller-Gallacher, J. L.; Nehme, R.; Warne, T.; Edwards, P. C.; Schertler, G. F.; Leslie, A. G.; Tate, C. G. The 2.1 A resolution structure of cyanopindolol-bound beta1-adrenoceptor identifies an intramembrane Na+ ion that stabilises the ligand-free receptor. *PLoS One* **2014**, *9* (3), e92727.

(4) Wang, S.; Wacker, D.; Levit, A.; Che, T.; Betz, R. M.; McCorvy, J. D.; Venkatakrishnan, A. J.; Huang, X. P.; Dror, R. O.; Shoichet, B. K.; et al. D4 dopamine receptor high-resolution structures enable the discovery of selective agonists. *Science* **2017**, *358* (6361), 381.

(5) Weinert, T.; Olieric, N.; Cheng, R.; Brunle, S.; James, D.; Ozerov, D.; Gashi, D.; Vera, L.; Marsh, M.; Jaeger, K.; et al. Serial millisecond crystallography for routine room-temperature structure determination at synchrotrons. *Nat. Commun.* **2017**, *8* (1), 542.

(6) Kang, Y.; Kuybeda, O.; de Waal, P. W.; Mukherjee, S.; Van Eps, N.; Dutka, P.; Zhou, X. E.; Bartesaghi, A.; Erramilli, S.; Morizumi, T.; et al. Cryo-EM structure of human rhodopsin bound to an inhibitory G protein. *Nature* **2018**, *558* (7711), 553.

(7) Velgy, N.; Hedger, G.; Biggin, P. C. GPCRs: What Can We Learn from Molecular Dynamics Simulations? *Methods Mol. Biol.* **2018**, *1705*, 133.

(8) Zhang, Y.; Sun, B.; Feng, D.; Hu, H.; Chu, M.; Qu, Q.; Tarrasch, J. T.; Li, S.; Sun Kobilka, T.; Kobilka, B. K.; et al. Cryo-EM structure of the activated GLP-1 receptor in complex with a G protein. *Nature* **2017**, *546* (7657), 248.

(9) Ernst, O. P.; Lodowski, D. T.; Elstner, M.; Hegemann, P.; Brown, L. S.; Kandori, H. Microbial and animal rhodopsins: structures, functions, and molecular mechanisms. *Chem. Rev.* **2014**, *114* (1), 126.

(10) Liu, W.; Chun, E.; Thompson, A. A.; Chubukov, P.; Xu, F.; Katritch, V.; Han, G. W.; Roth, C. B.; Heitman, L. H.; IJzerman, A. P.;

et al. Structural Basis for Allosteric Regulation of GPCRs by Sodium Ions. *Science* **2012**, *337* (6091), 232.
(11) Fenalti, G.; Giguere, P. M.; Katritch, V.; Huang, X. P.; Thompson, A. A.; Cherezov, V.; Roth, B. L.; Stevens, R. C. Molecular control of delta-opioid receptor signalling. *Nature* **2014**, *506*, 191.
(12) Yuan, S.; Hu, Z.; Filipek, S.; Vogel, H. W246$^{6.48}$ Opens a Gate for a Continuous Intrinsic Water Pathway during Activation of the Adenosine A Receptor. *Angew. Chem., Int. Ed.* **2014**, *54* (2), 556.
(13) Ericksen, S. S.; Cummings, D. F.; Weinstein, H.; Schetz, J. A. Ligand selectivity of D2 dopamine receptors is modulated by changes in local dynamics produced by sodium binding. *J. Pharmacol. Exp. Ther.* **2009**, *328* (1), 40.
(14) Yuan, S.; Vogel, H.; Filipek, S. The Role of Water and Sodium Ions in the Activation of the mu-Opioid Receptor. *Angew. Chem., Int. Ed.* **2013**, *52* (38), 10112.
(15) Cong, X.; Golebiowski, J. Allosteric Na(+)-binding site modulates CXCR4 activation. *Phys. Chem. Chem. Phys.* **2018**, *20* (38), 24915.
(16) Miao, Y.; Caliman, A. D.; McCammon, J. A. Allosteric effects of sodium ion binding on activation of the m3 muscarinic g-protein-coupled receptor. *Biophys. J.* **2015**, *108* (7), 1796.
(17) Makman, M. H.; Dvorkin, B.; Klein, P. N. Sodium ion modulates D2 receptor characteristics of dopamine agonist and antagonist binding sites in striatum and retina. *Proc. Natl. Acad. Sci. U. S. A.* **1982**, *79* (13), 4212.
(18) Watanabe, M.; George, S. R.; Seeman, P. Regulation of anterior pituitary D2 dopamine receptors by magnesium and sodium ions. *J. Neurochem.* **1985**, *45* (6), 1842.
(19) Ye, L.; Neale, C.; Sljoka, A.; Lyda, B.; Pichugin, D.; Tsuchimura, N.; Larda, S. T.; Pomes, R.; Garcia, A. E.; Ernst, O. P.; et al. Mechanistic insights into allosteric regulation of the A2A adenosine G protein-coupled receptor by physiological cations. *Nat. Commun.* **2018**, *9* (1), 1372.
(20) Draper-Joyce, C. J.; Verma, R. K.; Michino, M.; Shonberg, J.; Kopinathan, A.; Klein Herenbrink, C.; Scammells, P. J.; Capuano, B.; Abramyan, A. M.; Thal, D. M.; et al. The action of a negative allosteric modulator at the dopamine D2 receptor is dependent upon sodium ions. *Sci. Rep.* **2018**, *8* (1), 1208.
(21) Chien, E. Y. T.; Liu, W.; Zhao, Q.; Katritch, V.; Won Han, G.; Hanson, M. A.; Shi, L.; Newman, A. H.; Javitch, J. A.; Cherezov, V.; et al. Structure of the Human Dopamine D3 Receptor in Complex with a D2/D3 Selective Antagonist. *Science* **2010**, *330* (6007), 1091.
(22) Selley, D. E.; Cao, C.-C.; Liu, Q.; Childers, S. R. Effects of sodium on agonist efficacy for G-protein activation in μ-opioid receptor-transfected CHO cells and rat thalamus. *Br. J. Pharmacol.* **2000**, *130* (5), 987.
(23) Neve, K. A. Regulation of dopamine D2 receptors by sodium and pH. *Mol. Pharmacol.* **1991**, *39* (4), 570.
(24) Ananthanarayanan, V. S.; Kerman, A. Role of metal ions in ligand-receptor interaction: insights from structural studies. *Mol. Cell. Endocrinol.* **2006**, *246* (1−2), 53.
(25) Strasser, A.; Wittmann, H. J.; Schneider, E. H.; Seifert, R. Modulation of GPCRs by monovalent cations and anions. *Naunyn-Schmiedeberg's Arch. Pharmacol.* **2015**, *388* (3), 363.
(26) Gulya, K.; Kova′cs, G. L.; Ka′sa, P. Regulation of endogenous calcium and magnesium levels by δ opioid receptors in the rat brain. *Brain Res.* **1991**, *547* (1), 32.
(27) Tejwani, G. A.; Hanissian, S. H. Modulation of mu, delta and kappa opioid receptors in rat brain by metal ions and histidine. *Neuropharmacology* **1990**, *29* (5), 445.
(28) Wang, S.; Che, T.; Levit, A.; Shoichet, B. K.; Wacker, D.; Roth, B. L. Structure of the D2 dopamine receptor bound to the atypical antipsychotic drug risperidone. *Nature* **2018**, *555* (7695), 269.
(29) Free, R. B.; Chun, L. S.; Moritz, A. E.; Miller, B. N.; Doyle, T. B.; Conroy, J. L.; Padron, A.; Meade, J. A.; Xiao, J.; Hu, X.; et al. Discovery and characterization of a G protein-biased agonist that inhibits beta-arrestin recruitment to the D2 dopamine receptor. *Mol. Pharmacol.* **2014**, *86* (1), 96.
(30) Li, J.; Jonsson, A. L.; Beuming, T.; Shelley, J. C.; Voth, G. A. Ligand-dependent activation and deactivation of the human adenosine A(2A) receptor. *J. Am. Chem. Soc.* **2013**, *135* (23), 8749.
(31) White, K. L.; Eddy, M. T.; Gao, Z.-G.; Han, G. W.; Lian, T.; Deary, A.; Patel, N.; Jacobson, K. A.; Katritch, V.; Stevens, R. C. Structural Connection between Activation Microswitch and Allosteric Sodium Site in GPCR Signaling. *Structure* **2018**, *26* (2), 259.
(32) Newton, C. L.; Wood, M. D.; Strange, P. G. Examining the Effects of Sodium Ions on the Binding of Antagonists to Dopamine D2 and D3 Receptors. *PLoS One* **2016**, *11* (7), e0158808.
(33) Michino, M.; Free, R. B.; Doyle, T. B.; Sibley, D. R.; Shi, L. Structural basis for Na(+)-sensitivity in dopamine D2 and D3 receptors. *Chem. Commun.* **2015**, *51* (41), 8618.
(34) Vickery, O. N.; Carvalheda, C. A.; Zaidi, S. A.; Pisliakov, A. V.; Katritch, V.; Zachariae, U. Intracellular Transfer of Na(+) in an Active-State G-Protein-Coupled Receptor. *Structure* **2018**, *26* (1), 171.
(35) Vass, M.; Kooistra, A. J.; Ritschel, T.; Leurs, R.; de Esch, I. J.; de Graaf, C. Molecular interaction fingerprint approaches for GPCR drug discovery. *Curr. Opin. Pharmacol.* **2016**, *30*, 59.
(36) Singh, J.; Deng, Z.; Narale, G.; Chuaqui, C. Structural interaction fingerprints: a new approach to organizing, mining, analyzing, and designing protein-small molecule complexes. *Chem. Biol. Drug Des.* **2006**, *67* (1), 5.
(37) Deng, Z.; Chuaqui, C.; Singh, J. Structural interaction fingerprint (SIFt): a novel method for analyzing three-dimensional protein-ligand binding interactions. *J. Med. Chem.* **2004**, *47* (2), 337.
(38) Chan, H. C. S.; Wang, J.; Palczewski, K.; Filipek, S.; Vogel, H.; Liu, Z.-J.; Yuan, S. Exploring a new ligand binding site of G protein-coupled receptors. *Chemical Science* **2018**, *9*, 6480.
(39) Kling, R. C.; Clark, T.; Gmeiner, P. Comparative MD Simulations Indicate a Dual Role for Arg1323.50 in Dopamine-Dependent D2R Activation. *PLoS One* **2016**, *11* (1), e0146612.
(40) Kling, R. C.; Tschammer, N.; Lanig, H.; Clark, T.; Gmeiner, P. Active-state model of a dopamine D2 receptor-Galphai complex stabilized by aripiprazole-type partial agonists. *PLoS One* **2014**, *9* (6), e100069.
(41) Huang, W.; Manglik, A.; Venkatakrishnan, A. J.; Laeremans, T.; Feinberg, E. N.; Sanborn, A. L.; Kato, H. E.; Livingston, K. E.; Thorsen, T. S.; Kling, R. C.; et al. Structural insights into micro-opioid receptor activation. *Nature* **2015**, *524* (7565), 315.
(42) Kroeze, W. K.; Sassano, M. F.; Huang, X.-P.; Lansu, K.; McCorvy, J. D.; Giguere, P. M.; Sciaky, N.; Roth, B. L. PRESTO-Tango as an open-source resource for interrogation of the druggable human GPCRome. *Nat. Struct. Mol. Biol.* **2015**, *22* (5), 362.
(43) Eswar, N.; Webb, B.; Marti-Renom, M. A.; Madhusudhan, M. S.; Eramian, D.; Shen, M. Y.; Pieper, U.; Sali, A. Comparative protein structure modeling using MODELLER. *Current protocols in protein science* **2007**, *50*, 2.9.1.
(44) Mandell, D. J.; Coutsias, E. A.; Kortemme, T. Sub-angstrom accuracy in protein loop reconstruction by robotics-inspired conformational sampling. *Nat. Methods* **2009**, *6* (8), 551.
(45) Shivakumar, D.; Williams, J.; Wu, Y. J.; Damm, W.; Shelley, J.; Sherman, W. Prediction of Absolute Solvation Free Energies using Molecular Dynamics Free Energy Perturbation and the OPLS Force Field. *J. Chem. Theory Comput.* **2010**, *6* (5), 1509.
(46) Sondergaard, C. R.; Olsson, M. H. M.; Rostkowski, M.; Jensen, J. H. Improved Treatment of Ligands and Coupling Effects in Empirical Calculation and Rationalization of pK(a) Values. *J. Chem. Theory Comput.* **2011**, *7* (7), 2284.
(47) Zarzycka, B.; Zaidi, S. A.; Roth, B. L.; Katritch, V. Harnessing Ion-Binding Sites for GPCR Pharmacology. *Pharmacol. Rev.* **2019**, *71* (4), 571.
(48) Greenwood, J. R.; Calkins, D.; Sullivan, A. P.; Shelley, J. C. Towards the comprehensive, rapid, and accurate prediction of the favorable tautomeric states of drug-like molecules in aqueous solution. *J. Comput.-Aided Mol. Des.* **2010**, *24* (6−7), 591.
(49) Wolf, M. G.; Hoefling, M.; Aponte-Santamaria, C.; Grubmuller, H.; Groenhof, G. g_membed: Efficient insertion of a membrane

https://dx.doi.org/10.1021/acscentsci.9b01247
ACS Cent. Sci. 2020, 6, 274−282

protein into an equilibrated lipid bilayer with minimal perturbation. *J. Comput. Chem.* **2010**, *31* (11), 2169.
(50) Lomize, A. L.; Pogozheva, I. D.; Mosberg, H. I. Anisotropic solvent model of the lipid bilayer. 1. Parameterization of long-range electrostatics and first solvation shell effects. *J. Chem. Inf. Model.* **2011**, *51* (4), 918.
(51) Klauda, J. B.; Venable, R. M.; Freites, J. A.; O'Connor, J. W.; Tobias, D. J.; Mondragon-Ramirez, C.; Vorobyov, I.; MacKerell, A. D.; Pastor, R. W. Update of the CHARMM All-Atom Additive Force Field for Lipids: Validation on Six Lipid Types. *J. Phys. Chem. B* **2010**, *114* (23), 7830.
(52) Vanommeslaeghe, K.; Raman, E. P.; MacKerell, A. D., Jr. Automation of the CHARMM General Force Field (CGenFF) II: assignment of bonded parameters and partial atomic charges. *J. Chem. Inf. Model.* **2012**, *52* (12), 3155.
(53) Frisch, M. J.; Trucks, G. W.; Schlegel, H. B.; Scuseria, G. E.; Robb, M. A.; Cheeseman, J. R.; Scalmani, G.; Barone, V.; Mennucci, B.; Petersson, G. A.; Nakatsuji, H.; Caricato, M.; Li, X.; Hratchian, H. P.; Izmaylov, A. F.; Bloino, J.; Zheng, G.; Sonnenberg, J. L.; Hada, M.; Ehara, M.; Toyota, K.; Fukuda, R.; Hasegawa, J.; Ishida, M.; Nakajima, T.; Honda, Y.; Kitao, O.; Nakai, H.; Vreven, T.; Montgomery, Jr., J. A.; Peralta, J. E.; Ogliaro, F.; Bearpark, M.; Heyd, J. J.; Brothers, E.; Kudin, K. N.; Staroverov, V. N.; Kobayashi, R.; Normand, J.; Raghavachari, K.; Rendell, A.; Burant, J. C.; Iyengar, S. S.; Tomasi, J.; Cossi, M.; Rega, N.; Millam, J. M.; Klene, M.; Knox, J. E.; Cross, J. B.; Bakken, V.; Adamo, C.; Jaramillo, J.; Gomperts, R.; Stratmann, R. E.; Yazyev, O.; Austin, A. J.; Cammi, R.; Pomelli, C.; Ochterski, J. W.; Martin, R. L.; Morokuma, K.; Zakrzewski, V. G.; Voth, G. A.; Salvador, P.; Dannenberg, J. J.; Dapprich, S.; Daniels, A. D.; Farkas, Ö.; Foresman, J. B.; Ortiz, J. V.; Cioslowski, J.; Fox, D. J. *Gaussian 09*, Revision A.1; Gaussian, Inc.: Wallingford CT, 2009.
(54) Pronk, S.; Pall, S.; Schulz, R.; Larsson, P.; Bjelkmar, P.; Apostolov, R.; Shirts, M. R.; Smith, J. C.; Kasson, P. M.; van der Spoel, D.; et al. GROMACS 4.5: a high-throughput and highly parallel open source molecular simulation toolkit. *Bioinformatics* **2013**, *29* (7), 845.
(55) Jo, S.; Kim, T.; Iyer, V. G.; Im, W. CHARMM-GUI: a web-based graphical user interface for CHARMM. *J. Comput. Chem.* **2008**, *29* (11), 1859.
(56) Yuan, S.; Chan, H. C.; Filipek, S.; Vogel, H. PyMOL and Inkscape Bridge the Data and the Data Visualization. *Structure* **2016**, *24* (12), 2041.
(57) Adams, P. D.; Afonine, P. V.; Bunkoczi, G.; Chen, V. B.; Davis, I. W.; Echols, N.; Headd, J. J.; Hung, L. W.; Kapral, G. J.; Grosse-Kunstleve, R. W.; et al. PHENIX: a comprehensive Python-based system for macromolecular structure solution. *Acta Crystallogr., Sect. D: Biol. Crystallogr.* **2010**, *66* (Pt 2), 213.
(58) Emsley, P.; Lohkamp, B.; Scott, W. G.; Cowtan, K. Features and development of Coot. *Acta Crystallogr., Sect. D: Biol. Crystallogr.* **2010**, *66* (4), 486.
(59) Bochevarov, A. D.; Harder, E.; Hughes, T. F.; Greenwood, J. R.; Braden, D. A.; Philipp, D. M.; Rinaldo, D.; Halls, M. D.; Zhang, J.; Friesner, R. A. Jaguar: A high-performance quantum chemistry software program with strengths in life and materials sciences. *Int. J. Quantum Chem.* **2013**, *113* (18), 2110.
(60) *Schrödinger*; Schrödinger, LLC, 2018.

NOTE ADDED AFTER ASAP PUBLICATION

This paper was originally published ASAP on January 23, 2020. The title was corrected, and the paper reposted on January 24, 2020.

https://dx.doi.org/10.1021/acscentsci.9b01247
ACS Cent. Sci. 2020, 6, 274−282